Published in final edited form as:
J Neurosci. 2011 January 19; 31(3): 1017–1022. doi:10.1523/JNEUROSCI.4731-10.2011.

Dendritic calcium activity precedes inspiratory bursts in preBötzinger Complex neurons

Christopher A. Del Negro[1], **John A. Hayes**[1,§], and **Jens C. Rekling**[2]

Jens C. Rekling: jrekling@sund.ku.dk

[1] Department of Applied Science, McGlothlin-Street Hall, The College of William & Mary, Williamsburg, Virginia, USA

[2] Department of Neuroscience and Pharmacology, Panum Institute, Copenhagen DK-2200, Denmark. Tel: +45 35 32 74 64, Fax: +45 35 32 75 37

Abstract

Medullary interneurons of the preBötzinger Complex (preBötC) assemble excitatory networks that produce inspiratory related neural rhythms, but the importance of somatodendritic conductances in rhythm generation is still incompletely understood. Synaptic input may cause Ca^{2+} accumulation post-synaptically to evoke a Ca^{2+}-activated inward current that contributes to inspiratory burst generation. We measured Ca^{2+} transients by two-photon imaging dendrites while recording neuronal somata electrophysiologically. Dendritic Ca^{2+} accumulation frequently precedes inspiratory bursts, particularly at recording sites 50–300 μm distal from the soma. Pre-inspiratory Ca^{2+} transients occur in 'hotspots', not ubiquitously, in dendrites. Ca^{2+} activity propagates orthodromically toward the soma (and antidromically to more distal regions of the dendrite), at rapid rates (300–700 μm/s). These high propagation rates suggest that dendritic Ca^{2+} activates an inward current to electrotonically depolarize the soma, rather than propagate as a regenerative Ca^{2+} wave. These data provide new evidence that respiratory rhythmogenesis may depend on dendritic burst-generating conductances activated in the context of network activity.

INTRODUCTION

Breathing behavior in mammals depends on inspiratory neural rhythms that originate in the preBötzinger Complex (preBötC) of the ventral medulla. Glutamatergic interneurons comprise its rhythmogenic core and a key unsolved question pertains to the spatiotemporal distribution of active conductances in the somatodendritic membrane and their role in rhythmogenesis (Ramirez et al., 2004; Feldman and Del Negro, 2006). One possible mechanism posits that recurrent synaptic interactions evoke postsynaptic conductances to generate inspiratory bursts (Rekling et al., 1996; Rekling and Feldman, 1998). Specifically, recurrent excitation may elevate postsynaptic Ca^{2+} and thus activate nonspecific cationic current (I_{CAN}) (Mironov, 2008; Rubin et al., 2009). Studies in a slice model of respiratory rhythm show that I_{CAN} is one important charge carrier underlying inspiratory bursts (Thoby-

Correspondence: Christopher A. Del Negro, Ph.D., September 2010 – May 2011, Institut de Neurobiologie Alfred Fessard, Neurobiologie et Développement, Centre National de la Recherche Scientifique, Av, de la terrasse, 91198 Gif-sur-Yvette, France, Lab tel: +33 (0) 1 69 82 34 49, Mobile: +33 (0) 6 49 20 78 55.

§Present address: Institut de Neurobiologie Alfred Fessard, Neurobiologie et Développement Centre National de la Recherche Scientifique, Gif-sur-Yvette, France. Tel: +33 (0) 1 69 82 34 55, Fax: +33 (0) 1 69 82 41 78, john.hayes@inaf.cnrs-gif.fr.

Permanent address: McGlothlin-Street Hall, Room 318, The College of William & Mary, Williamsburg, Virginia 23187-8795, USA, 757-221-7808 (office), 757-221-7749 (lab), 757-221-2050 (fax), cadeln@wm.edu

Brisson and Ramirez, 2001; Pena et al., 2004), and that the synaptic recruitment of I_{CAN} takes place in the dendrites (Pace et al., 2007b; Mironov, 2008).

Glutamatergic preBötC neurons have the potential to excite their postsynaptic targets and thus cause Ca^{2+} to accumulate in the dendrites prior to inspiratory bursts. This has been examined in slices and organotypic cultures but recording sites were limited to proximal dendrites (~50 μm from the soma) and many data were acquired from non-rhythmic cultures (Mironov, 2008; 2009). Therefore, the extent to which these data apply to preBötC neuron dendrites in the context of rhythmogenesis remains uncertain. We measured post-synaptic Ca^{2+} dynamics in soma-close and soma-distal dendritic locations, using acute slices that retain respiratory function *in vitro*. We show that endogenous synaptic drive evokes dendritic Ca^{2+} transients prior to somatic inspiratory bursts, which suggests that synaptically activated dendritic conductances may influence respiratory rhythm generation.

METHODS

The Institutional Animal Care and Use Committee at the College of William & Mary and the Danish National Committee for Ethics in Animal Research approved all procedures. Neonatal mice (P0-6) were dissected in artificial cerebrospinal fluid (ACSF) containing (in mM): 124 NaCl, 3 KCl, 1.5 $CaCl_2$, 1 $MgSO_4$, 25 $NaHCO_3$, 0.5 NaH_2PO_4, and 30 dextrose, equilibrated with 95% O_2-5% CO_2 (pH 7.4). $CaCl_2$ was adjusted to 1.1 mM in some experiments (see below). We cut 550-μm-thick transverse slices that expose the preBötC at the rostral face (Ruangkittisakul et al., 2010) Slices were perfused with 27°C oxygenated ACSF at 4 ml/min. The K^+ concentration ($[K^+]_o$) was raised to 9 mM in ACSF containing 1.5 mM $CaCl_2$. The $[K^+]_o$ was raised to 5 mM in ACSF containing 1.1 mM $CaCl_2$. In both cases the tradeoff of raising $[K^+]_o$ toward a maximum of 9 mM, and lowering $[Ca^{2+}]_o$ toward a minimum of 1 mM, maintains excitability and sustains rhythmic function (Ruangkittisakul et al., 2007). Motor output was recorded from hypoglossal (XII) nerve roots.

Infrared-enhanced differential interference contrast (IR-DIC) videomicroscopy was performed using a Zeiss fixed-stage microscope with Köhler illumination and a 20x/1.0 NA objective (Carl Zeiss, Thornwood, NY).

We performed whole-cell recordings using an EPC-10 amplifier (HEKA, Bellmore, NY). Data were filtered at 1 kHz and acquired at 10 kHz. Standard patch solution contained (in mM): 140 K-Gluconate, 10 NaCl, 0.5 $CaCl_2$, 10 HEPES, 1 EGTA, 2 Mg-ATP, and 0.3 Na3-GTP (pH 7.3). We added 200 μM Oregon Green 488 BAPTA-2 (OGB-2, K_d=580 nM) and 50 μM Alexa 568 hydrazide (Invitrogen, Carlsbad, CA) prior to use.

We performed two-photon imaging using a Ti:Sapphire laser (Spectra Physics, Newport, CA) in conjunction with a laser-scanning microscope (Zeiss). Images were acquired by non-descanned detectors at 20 Hz.

We gated image-acquisition protocols via logic pulses from the EPC-10. Gating pulses were recorded at 10 kHz in a separate channel of the chart recorder along with logic pulses returned by the LSM 510 upon the initiation of the first (and last) scans of the time series. Return pulses were used to sync the electrophysiology data with the image stack.

We report 54 neurons recorded with 200 μM OGB-2. We varied the concentration and the affinity of the Ca^{2+} dye to discern optimal recording conditions, using 400 μM Oregon Green 488 BAPTA-1 (OGB-1, K_d=190 nM) and 100–500 μM Oregon Green 488 BAPTA-6F (OGB-6F, K_d=3 μM) in preliminary experiments. OGB-6F yielded fast-decaying somatic signals, but the low affinity of the dye diminished dendritic fluorescence.

OGB-1 was readily detectable in dendrites, but its long-lasting decay caused spurious temporal summation of fluorescence changes (ΔF). Figure 1D–F reports OGB-1 experiments wherein ΔF decayed to baseline during each respiratory cycle. The rise time was equally rapid for OGB-1, OGB-2, and OGB-6F.

Alexa 568 hydrazide dye in the patch solution enabled us to visualize the dendritic arbor within 5 min of establishing the whole-cell configuration. Three to six principle dendrites were always visible in preBötC neurons. OGB diffuses more slowly than Alexa 568 hydrazide, so we waited at least 20 min before measuring dendritic Ca^{2+} activity. After 20 min we recorded one principle dendrite per 10 min until whole-cell recording conditions deteriorated.

In eight experiments we imaged the soma and proximal dendrites of preBötC neurons loaded with membrane-permeable Ca^{2+} dye *in vitro*. Slices were loaded with Fluo-8™ AM (K_d=389 nM, AAT Bioquest, Sunnyvale, CA) via submersion for 60–90 min while bubbling with 95% O_2-5% CO_2. We dissolved 50 μg Fluo-8 AM in 50 μl DMSO, and then combined 20 μl of the Fluo-8 AM solution with 5 μl cremophore EL (Fluka, St. Louis, MO) and 5 μl of 20% Pluronic F-127 in DMSO. We added the 30 μl of Fluo-8 AM solution to 1 ml ACSF with 100 mM mannitol (Sigma-Aldrich, St. Louis, MO) and 100 μM MK-571 (Enzo Life Sciences, Farmingdale, NY). The final Fluo-8 AM concentration was 20 μM.

We imaged Fluo-8 AM-labeled neurons using an Olympus BX51 microscope (Tokyo, Japan) with a 63x/0.95 NA objective. Image stacks were acquired at 70 Hz using a CCD camera (Andor Technology, Belfast, UK).

Images were analyzed with ImageJ (NIH, Bethesda, MD). For each bout, we created a composite image showing the standard deviation of fluorescence through the image stack. This composite shows dendritic regions of interest (ROIs) with large ΔF, which often indicates periodicity. For each ROI, we plotted a histogram of fluorescence measurements and fitted a Gaussian function to determine the mean and standard deviation (SD). The mean reflects baseline fluorescence (F_0) and was used to normalize the ΔF signal, which was subsequently displayed as $\Delta F/F_0$. The SD was used to determine the onset of fluorescence 'bursts'. The first point in the $\Delta F/F_0$ signal to exceed baseline by ≥2 SD was considered statistically significant at $p<0.05$ and was defined as the dendritic fluorescence onset time (T_{DEN}). The onset time of the somatic burst (T_{SOMA}) was defined as the absolute time of maximum rate of rise (dV_M/dt) of the voltage, or the maximum rate of rise of somatic Ca^{2+} fluorescence. The inherent disparity in sampling rate and signal-to-noise ratio was the basis for defining T_{DEN} and T_{SOMA}. Cycle-triggered averages of inspiratory bursts were computed from ≥7 consecutive cycles based on a threshold-crossing algorithm applied to the XII output. Dendritic Ca^{2+} latency (ΔT) was defined as the difference between T_{DEN} and T_{SOMA}, ($\Delta T = T_{DEN} - T_{SOMA}$).

RESULTS

We recorded preBötC interneurons showing evidence of a build-up of presynaptic excitatory input and strong inspiratory bursts, including summating EPSPs, ramp-like depolarization and spike discharge at a low rate (2–10 Hz) during the expiratory phase, particularly 300–900 ms prior to XII output. Robust inspiratory bursts experience depolarization block (i.e., voltage-dependent spike inactivation), which attenuates intraburst spiking. We probed for these characteristics, which may indicate rhythmogenic function, during on-cell recording (Figs. 1A, 2A) as selection criteria for subsequent whole-cell recording.

The patch solution contained 2 mM QX-314 to prevent voltage-gated Ca^{2+} channels evoked during action potentials from obscuring synaptic-dendritic Ca^{2+} activity. QX-314 blocks

spiking intracellularly, but has no effect on network properties such as recurrent excitation, which can be detected as pre-inspiratory ramp-like voltage trajectory and temporal summation of EPSPs (Fig. 1B). Nevertheless, Ca^{2+} transients in the soma and proximal dendrites (20–50 μm) coincided with the somatic inspiratory drive potential (Fig. 1B,C).

We hypothesized that postsynaptic Ca^{2+} accumulation prior to somatic burst generation might be detectable in more distal dendrites. To quantify the temporal relationship of dendritic Ca^{2+} and somatic inspiratory bursts, we subtracted the onset time of the inspiratory drive potential (T_{SOMA}) from the fluorescence onset time in the dendrite (T_{DEN}) to obtain the dendritic Ca^{2+} latency (ΔT), which we dub *drive latency*. Figure 1D,E shows dendritic $\Delta F/F_0$ measured 90 μm from the soma. ΔT was less than zero in 75% of cycles measured, thus dendritic Ca^{2+} generally increased prior to the inspiratory drive potential. The average dendritic Ca^{2+} latency measured −12±8 ms, with a range of −6 to −34 ms (n=7 cycles at 90 μm), and −28±15 ms at an average distance of 76±15 μm in five dendritic branches (n=24 cycles in total).

These latency times are reliable, even though they are smaller than the sampling interval (49 ms/frame), because T_{DEN} was determined based on the first dendritic measurement to exceed baseline fluorescence by two or more SD; we did not interpolate between points to estimate T_{DEN}. This method of computing ΔT may underestimate the dendritic Ca^{2+} latency because if the sampling rate was higher, then a significant increase in dendritic Ca^{2+} fluorescence would be detectable earlier. The dendritic sampling rate has no effect on T_{SOMA}, which is determined by electrophysiology (10 kHz).

ΔT exceeded zero in two cycles marked by † in Fig. 1D (5 and 28 ms, respectively), which may reflect dendritic Ca^{2+} channel activity evoked electrotonically by somatic depolarization. To evaluate this possibility, we applied step-current commands 500 ms after the inspiratory burst, when network synaptic activity is minimal and few spontaneous synaptic potentials can be detected. The step command caused a significant dendritic fluorescence response within 38 ms (Fig. 1F), which was commensurate with inspiratory bursts in which ΔT was also positive and the dendritic $\Delta F/F_0$ occurred 5–28 ms after the inspiratory drive potential.

The peak dendritic fluorescence always occurred ~200 ms (or more) after the onset of the drive potential, even during respiratory cycles in which initial dendritic Ca^{2+} preceded the somatic burst ($\Delta T<0$, e.g., Fig. 1E). The dendritic fluorescence similarly peaked ~240 ms after the step command (Fig. 1F). These data suggest that the maximum dendritic Ca^{2+} response is attributable to voltage-gated Ca^{2+} channels evoked electrotonically by somatic depolarization.

A caveat is that QX-314 also enhances the amplitude of the inspiratory drive potential (Pace et al., 2007a). AMPA receptors ordinarily evoke Ca^{2+} channels (Pace and Del Negro, 2008), but the QX-314-amplified drive potential may artificially increase Ca^{2+} channel recruitment and cause one to overestimate the synaptically triggered Ca^{2+} activity. Therefore, we subsequently omitted QX-314 from the patch solution and concentrated on measuring dendritic Ca^{2+} latency.

Figure 2A–F shows a preBötC neuron recorded with K-Gluconate solution. Pre-inspiratory spiking was robust on-cell (Fig. 2A) so in whole-cell we applied negative bias to prevent intraburst spiking that would otherwise obscure our ability to measure synaptic Ca^{2+} activity. During inspiratory cycles, ΔT measured 87±13 ms at a site 220 μm from the cell body (n=22 cycles, ROI_1, Fig. 2B). The latency at ROI_1 was significantly longer in response to step current injection through the somatic patch electrode, 182±35 ms (n=5 pulse injections, Fig. 2C,F, $p<0.05$). This disparity suggests that a proximal dendritic site triggered

Ca^{2+} accumulation at ROI_1 during inspiratory cycles. To test this we recorded contiguous regions of the dendrite between ROI_1 and the soma. At a site 81 μm from the cell body ΔT measured −90±14 ms (n=23 cycles from ROI_2, Fig. 2D,E). Because ROI_1 and ROI_2 were separated by 139 μm, and T_{DEN} occurred 177 ms later at ROI_1, the data suggest that Ca^{2+} activity originating at or near ROI_2 influenced adjacent regions of the dendrite at a rate of ~785 μm/s.

We detected Ca^{2+} transients in the dendrite occurring both before and after the inspiratory burst in four experiments. Figure 2G shows a cycle-triggered average in a representative preBötC neuron. Distal sites such as ROI_1 and ROI_2 (154 and 94 μm from the soma, respectively) showed Ca^{2+} transients prior to the inspiratory phase, which propagated orthodromically at a rate in the range of 660–1000 μm/s. ROI_3 (57 μm from the soma) showed no evidence of Ca^{2+} activity prior to the inspiratory burst. Pre-inspiratory Ca^{2+} transients detected in the soma (ROI_4) were most likely attributable to pre-inspiratory spiking activity that we could not fully suppress via DC bias (Fig. 2H asterisks). These data suggest that not all sites in the dendrite are excitable and that pre-inspiratory Ca^{2+} activity occurs in specialized ‘hotspots’. Peak fluorescence always occurred after the onset of the inspiratory phase, which is equally clear in Figs. 1 and 2. Ca^{2+} transients that accompany the inspiratory burst occur synchronously throughout the dendrite, not in ‘hotspots’, and always peaked within ~200 ms of T_{SOMA} (Fig. 2H).

We measured dendritic Ca^{2+} latency at 20 dendritic ROIs in eight preBötC neurons loaded by simultaneously imaging the dendrites and soma, which circumvents whole-cell dialysis that can affect the Ca^{2+} dynamics in the soma and dendrites. A representative experiment shows ΔT of 34 ms for a dendritic site located 71 μm from the soma (Fig. 2I,J). ΔT measured less than zero in 17 dendritic sites 24–74 μm away from the soma, and was ~0 in three cases (Fig. 2K).

We plotted the entire set of dendritic Ca^{2+} latency measurements for endogenous inspiratory bursts and responses to step-current injection as a function of dendritic recording distance. These data include 36 recordings with K-Gluconate patch solution (Fig. 3A, red), 17 recordings with QX-314 included (Fig. 3A, green), 20 different dendritic sites in 8 neurons imaged at the soma and dendrite (Figs. 2K, 3A inset), and Ca^{2+} latency in response to step current injection from 20 neurons (Fig. 3B). Points below the origin reflect dendritic Ca^{2+} activity that precedes inspiratory burst generation. Points above the origin reflect Ca^{2+} activity evoked electrotonically as a result of somatic or local dendritic depolarization. Ca^{2+} activity was detected prior to somatic burst generation in most experiments. However, at recording sites less than 60 μm from the soma, ΔT often exceeded zero, suggesting dendritic Ca^{2+} attributable to the electrotonic effects of somatic depolarization. The step-current injections universally evoked positive dendritic Ca^{2+} latency, as expected.

DISCUSSION

The physiological properties of putatively rhythmogenic preBötC neurons – observed *in vivo* and *in vitro* over ~30 years – include a pre-inspiratory firing pattern and robust inspiratory bursts that experience intraburst depolarization block, which suggests the massive recruitment of inward current during inspiration (Richter, 1982; Rekling et al., 1996; Rekling and Feldman, 1998; Guyenet and Wang, 2001; Stornetta et al., 2003; Hayes and Del Negro, 2007; Rubin et al., 2009; Gray et al., 2010). We examined the Ca^{2+} signaling in dendrites to elucidate how the build-up of excitatory synaptic input evokes burst-generating conductances. In this study, the membrane properties of the presynaptic neurons remain unknown and could include a wide variety of discharge phenotypes, including neurons with bursting-pacemaker properties and intrinsic spiking activity, as well as neurons that

participate in recurrent excitatory clusters. However, all the presynaptic neurons share a propensity to increase their activity during the early inspiratory phase.

We recorded preBötC neurons based on pre-inspiratory firing pattern and depolarization block (Figs. 1A, 2A), which strongly suggests glutamatergic phenotype (Gray et al., 2010). The other major subpopulations in the preBötC are inhibitory interneurons that display low-amplitude inspiratory bursts (<5 mV) without pre-inspiratory firing (Kuwana et al., 2006;Winter et al., 2009).

Mironov documented dendritic waves of Ca^{2+}-induced Ca^{2+}-release (CICR) propagating at 72 μm/s, triggered by metabotropic glutamate receptors in preBötC neurons (Mironov, 2008; 2009). The ability to generate CICR waves may develop in culture, or it may be limited to the proximal dendrite, because we never detected similar Ca^{2+} waves in acute rhythmically active slices. We also recorded dendritic Ca^{2+} transients prior to somatic bursts, but not in every case. Ca^{2+} transients preceded somatic inspiratory bursts in 55 out of 74 experiments (74%). In general, the more distal the recording site, the earlier we detected Ca^{2+} signals. What propagates from dendrite to soma: Ca^{2+} or voltage? CICR generally propagates at ~70 μm/s in dendrites (Augustine et al., 2003). Alternatively, Ca^{2+} may evoke I_{CAN} at or near the synapse to depolarize the soma (and neighboring regions of dendrite) electrotonically. Cable theory shows that voltage changes propagate faster than CICR by orders of magnitude in neuronal dendrites. Since we did not detect Ca^{2+} waves per se, propagation reflects a quotient wherein the numerator is the distance between two recording sites, and the denominator is the temporal disparity of burst onset at each site. According to this definition, we recorded propagation rates of 300–700 μm/s, which is consistent with electrotonic propagation rather than CICR.

Dendritic Ca^{2+} transients originated after or in sync with somatic bursts or drive potentials in 19 of 74 experiments (26%). Here too, the antidromic propagation rates were 300–700 μm/s. Similar antidromic propagation rates were obtained in response to somatic step-current injections (Fig. 3B). The fact that their propagation rate is of similar magnitude (but opposite sign) to cycles with negative dendritic Ca^{2+} latency suggests that electrotonic factors govern the dendritic-somatic interactions in the preBötC in both orthodromic and antidromic responses. The data also suggest that some dendrites may receive very little or no drive at all, but still show Ca^{2+} activity by back propagating electrotonic effects.

We also detected dendritic sites with negative drive latency while neighboring regions of the dendrite, both proximal and distal, showed either no Ca^{2+} activity (Fig. 2G,H ROI_3) or positive drive latency (Fig. 2B,C,E ROI_1). These data indicate that synaptic drive leading to postsynaptic Ca^{2+} elevation occurs in hotspots, which presumably indicates points at or near excitatory synaptic contacts. Sites with positive drive latency reflect Ca^{2+} channels activated electrotonically from the soma, or neighboring regions of the dendrite, which again suggests electrotonic interactions among the dendrites and soma rather than CICR.

According to the group-pacemaker model, preBötC interneurons mutually interact to elevate postsynaptic Ca^{2+}, activate the inward current I_{CAN}, and periodically generate inspiratory bursts (Rekling et al., 1996; Rekling and Feldman, 1998; Mironov, 2008; Rubin et al., 2009). The relative timing of dendritic Ca^{2+} transients and somatic voltage changes is one measurable link between network-mediated synaptic drive and postsynaptic mechanisms that activate I_{CAN} (Morgado-Valle et al., 2008). Although these data affirm the key prediction that postsynaptic Ca^{2+} transients be detectable prior to somatic bursts – they do not prove that respiratory rhythm is group-pacemaker driven. Nor can these data rule out alternative models that emphasize voltage-dependent conductances such as persistent Na^+ current in rhythm generation (Koizumi and Smith, 2008). Regardless of whether emergent

network properties constitute the core mechanism of respiratory rhythmogenesis, as the group-pacemaker model postulates, the synaptic activation of I_{CAN} contributes substantially to inspiratory burst generation (Johnson et al., 2007; Pace et al., 2007b) and is relevant to understanding the neural origins of respiratory rhythm.

We conclude that synaptic input typically triggers Ca^{2+} accumulation in dendrites prior to burst generation. Our measurements are inconsistent with regenerative Ca^{2+} propagation from dendrite to soma, which is a relatively slow process (~70 μm/s) and unlikely to promote synaptic integration in the context of network rhythms. For example, consider an excitatory input 250 μm from the cell body. A CICR-dependent Ca^{2+} wave would require 3.5 s to influence the soma. In slices or *en bloc* preparations *in vitro*, the typical respiratory period is ~5 s. Synaptic inputs located 500 μm (or farther) from the soma would be impractically sited to influence somatic integration during a typical respiratory cycle. Moreover, the slow propagation rate of CICR would prevent spatial and temporal summation of excitatory synaptic inputs that occur simultaneously at multiple positions in the dendritic arbor. Instead, synaptic inputs may elevate Ca^{2+}, evoke I_{CAN}, and depolarize the dendrite locally. These 'hotspots' could thus act electrotonically to influence other regions of the dendrite and the soma in support of inspiratory burst generation. With propagation rates of 300–700 μm/s, it would be reasonable for multiple dendritic sites to undergo temporal and spatial summation of inputs during a typical respiratory cycle *in vitro*, and even during breathing cycles *in vivo* in which cycle period is typically less than 1 s in rodents.

Acknowledgments

GRANTS

R01-HL104127-01 (CDN, JAH); The Danish Medical Council, the NovoNordisk Foundation, Den Owensenske Fond, Lægeforeningens forskningsfond, and Agnes og Pouls Friis Fond (JCR).

References

Augustine GJ, Santamaria F, Tanaka K. Local calcium signaling in neurons. Neuron. 2003; 40:331–346. [PubMed: 14556712]

Feldman JL, Del Negro CA. Looking for inspiration: new perspectives on respiratory rhythm. Nat Rev Neurosci. 2006; 7:232–242. [PubMed: 16495944]

Gray PA, Hayes JA, Ling G, Llona I, Tupai S, CPM, Ross S, Hirata T, Corbin JG, Eugenin J, Del Negro CA. Developmental Origin of preBötzinger Complex Respiratory Neurons. J Neurosci. 2010 in press.

Guyenet PG, Wang H. Pre-Bötzinger neurons with preinspiratory discharges "in vivo" express NK1 receptors in the rat. J Neurophysiol. 2001; 86:438–446. [PubMed: 11431523]

Hayes JA, Del Negro CA. Neurokinin Receptor-Expressing PreBötzinger Complex Neurons in Neonatal Mice Studied In Vitro. J Neurophysiol. 2007; 97:4215–4224. [PubMed: 17409172]

Johnson SM, Wiegel LM, Majewski DJ. Are pacemaker properties required for respiratory rhythm generation in adult turtle brain stems in vitro? Am J Physiol Regul Integr Comp Physiol. 2007; 293:R901–910. [PubMed: 17522127]

Koizumi H, Smith JC. Persistent Na+ and K+-dominated leak currents contribute to respiratory rhythm generation in the pre-Bötzinger complex in vitro. J Neurosci. 2008; 28:1773–1785. [PubMed: 18272697]

Kuwana S, Tsunekawa N, Yanagawa Y, Okada Y, Kuribayashi J, Obata K. Electrophysiological and morphological characteristics of GABAergic respiratory neurons in the mouse pre-Botzinger complex. Eur J Neurosci. 2006; 23:667–674. [PubMed: 16487148]

Mironov S. Respiratory circuits: function, mechanisms, topology, and pathology. Neuroscientist. 2009; 15:194–208. [PubMed: 19307425]

Mironov SL. Metabotropic glutamate receptors activate dendritic calcium waves and TRPM channels which drive rhythmic respiratory patterns in mice. J Physiol. 2008; 586:2277–2291. [PubMed: 18308826]

Morgado-Valle C, Beltran-Parrazal L, DiFranco M, Vergara JL, Feldman JL. Somatic Ca2+ transients do not contribute to inspiratory drive in preBötzinger Complex neurons. J Physiol. 2008; 586:4531–4540. [PubMed: 18635649]

Pace RW, Del Negro CA. AMPA and metabotropic glutamate receptors cooperatively generate inspiratory-like depolarization in mouse respiratory neurons in vitro. Eur J Neurosci. 2008; 28:2434–2442. [PubMed: 19032588]

Pace RW, Mackay DD, Feldman JL, Del Negro CA. Role of persistent sodium current in mouse preBotzinger Complex neurons and respiratory rhythm generation. J Physiol. 2007a; 580:485–496. [PubMed: 17272351]

Pace RW, Mackay DD, Feldman JL, Del Negro CA. Inspiratory bursts in the preBötzinger Complex depend on a calcium-activated nonspecific cationic current linked to glutamate receptors. J Physiol. 2007b; 582:113–125. [PubMed: 17446214]

Pena F, Parkis MA, Tryba AK, Ramirez JM. Differential Contribution of Pacemaker Properties to the Generation of Respiratory Rhythms during Normoxia and Hypoxia. Neuron. 2004; 43:105–117. [PubMed: 15233921]

Ramirez JM, Tryba AK, Pena F. Pacemaker neurons and neuronal networks: an integrative view. Curr Opin Neurobiol. 2004; 14:665–674. [PubMed: 15582367]

Rekling JC, Feldman JL. PreBötzinger complex and pacemaker neurons: hypothesized site and kernel for respiratory rhythm generation. Annu Rev Physiol. 1998; 60:385–405. [PubMed: 9558470]

Rekling JC, Champagnat J, Denavit-Saubie M. Electroresponsive properties and membrane potential trajectories of three types of inspiratory neurons in the newborn mouse brain stem in vitro. J Neurophysiol. 1996; 75:795–810. [PubMed: 8714653]

Richter DW. Generation and maintenance of the respiratory rhythm. J Exp Biol. 1982; 100:93–107. [PubMed: 6757372]

Ruangkittisakul A, Panaitescu B, Ballanyi K. K+ and Ca2+ dependence of inspiratory-related rhythm in novel “calibrated” mouse brainstem slices. Respir Physiol Neurobiol. 2010 in press.

Ruangkittisakul A, Secchia L, Bornes TD, Palathinkal DM, Ballanyi K. Dependence on extracellular Ca2+/K+ antagonism of inspiratory centre rhythms in slices and en bloc preparations of newborn rat brainstem. J Physiol. 2007; 584:489–508. [PubMed: 17717009]

Rubin JE, Hayes JA, Mendenhall JL, Del Negro CA. Calcium-activated nonspecific cation current and synaptic depression promote network-dependent burst oscillations. Proc Natl Acad Sci U S A. 2009; 106:2939–2944. [PubMed: 19196976]

Stornetta RL, Sevigny CP, Guyenet PG. Inspiratory augmenting bulbospinal neurons express both glutamatergic and enkephalinergic phenotypes. J Comp Neurol. 2003; 455:113–124. [PubMed: 12455000]

Thoby-Brisson M, Ramirez JM. Identification of two types of inspiratory pacemaker neurons in the isolated respiratory neural network of mice. J Neurophysiol. 2001; 86:104–112. [PubMed: 11431492]

Winter SM, Fresemann J, Schnell C, Oku Y, Hirrlinger J, Hulsmann S. Glycinergic interneurons are functionally integrated into the inspiratory network of mouse medullary slices. Pflugers Arch. 2009; 458:459–469. [PubMed: 19238427]

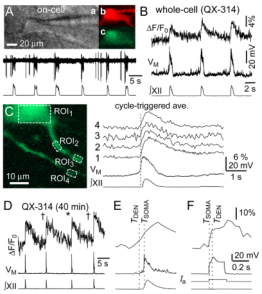

Figure 1.

Ca^{2+} measurements in preBötC neurons recorded with QX-314. **A**, IR-DIC videomicroscopy (a), Alexa 568 (b), and OGB-2 (c) images with on-cell recording (upper) and XII output (lower). **B**, imaging and electrophysiology from cell in A. **C**, cycle-triggered average of Ca^{2+} and membrane potential from cell in A,B. Vertical line indicates inspiratory onset. Numbered traces correspond to ROIs in the image. **D**, in a different cell, dendritic imaging 91 μm from the soma. Cycles marked with † show positive dendritic Ca^{2+} latency, cycle marked with * shows negative drive latency. **E**, cycle marked * displayed at higher sweep speed. F, dendritic and somatic responses to current injection. Broken lines indicate the T_{DEN} and T_{SOMA}.

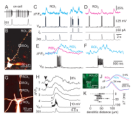

Figure 2.

Dendritic Ca^{2+} measurements in preBötC neurons recorded with standard K-Gluconate patch solution. **A**, on-cell recording and XII output. **B**, image of the cell in A (Alexa 568). **C** and **D**, dendritic Ca^{2+} dynamics in ROI_1 (C) and ROI_2 (D) with whole-cell and XII recordings. Step commands were applied while imaging ROI_1 in C. Vertical calibration bars apply to C–F. **E**, the first cycles from C and D re-plotted and superimposed at higher sweep speed. **F**, second evoked response from C re-plotted at higher sweep speed. **G**, image of a different preBötC neuron (Alexa 568). **H**, cycle-triggered average of somatodendritic activity. Imaging sweeps for ROIs 1–4 with membrane potential and XII output. Asterisks indicate somatic action potentials that evoked Ca^{2+} transients. Arrowheads (top traces) indicate negative dendritic Ca^{2+} latency. **I–K,** Ca^{2+} imaging from soma and dendrites. **I**, epifluorescence image. **J**, imaging sweeps showing raw and differentiated traces. **K**, dendritic Ca^{2+} latency versus recording distance for 20 dendritic recording sites. Horizontal error bars indicate the length of the dendritic ROI.

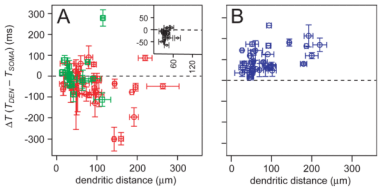

Figure 3.

Plots of dendritic Ca^{2+} latency versus recording distance for the entire data set. **A**, Drive latency for endogenous cycles of respiratory activity (red shows K-Gluconate recordings, green shows QX-314 experiments). Inset reproduces Fig. 2K. **B**, Dendritic Ca^{2+} latency in response to step commands (blue). Vertical error bars correspond to standard error of ΔT. Horizontal error bars indicate the length of the dendritic ROI.